

Magneto: A Versatile Multi-Limbed Inspection Robot

Tirthankar Bandyopadhyay, Ryan Steindl, Fletcher Talbot, Navinda Kottege,
Ross Dungavell, Brett Wood, James Barker, Karsten Hoehn, Alberto Elfes

Abstract—In this paper we present the design and control strategies of a novel quadruped climbing robot (named Magneto) with three degrees of freedom (3-DOF) actuated limbs and a 3-DOF compliant magnetic foot. By exploiting its high degrees of freedom, Magneto is able to deform its body shape to squeeze through gaps of 23cm, which is smaller than standard human entry portholes of industrial confined spaces. Its compact foot design of footprint 4cm allows Magneto to walk on narrow beams of thickness less than 5cm, even at varying separation. The inherent high dimensional system design enables the body to be positioned in a wide range of orientations and seamlessly switch a limb function from locomotion to manipulation mode mid-climb. This capability enables access to confined space openings and occluded pockets and navigation through complex 3-D structures previously not demonstrated on legged climbing robots.

I. INTRODUCTION

Robots for industrial inspection are increasingly being used to reduce human risk and effort in obtaining structural integrity information. While there are many solutions for remote visual inspections using aerial platforms [1], such methods often suffer from occlusion induced coverage gaps, especially in confined and narrow spaces. In addition, close-range visual inspection and many non destructive techniques like ultrasonic testing, eddy-current testing, acoustic emission testing, *etc.* require the sensor to be in close proximity or be in surface contact during measurement. Long term sensing using aerial platforms in complex 3-D structures for such tasks becomes extremely challenging. Climbing robots, being able to address these constraints relatively easily, have invoked renewed interest as a mode of effective infrastructure inspection solution.

Different adhesion modalities have been explored for climbing a variety of surfaces: suction cups [2]–[4], micro-spines [5], [6], micro-fibrillar based gecko feet [7], [8], permanent magnetic [9] as well as electro-magnetic adhesion [10]. Grasping mechanisms have also been explored to traverse thin beams and structural cables as shown in [11]. In the domain of industrial and maritime infrastructure, magnetic adhesion is generally preferred due to the presence of ferrous alloys in most structural components. Additionally, a key inspection task is the detection of corrosion and paint quality of such ferrous structures making magnetic adhesion a primary mode of choice for robots climbing in such an environment. The quadruped robot, presented in this paper, is developed for such tasks and uses a permanent-electromagnet for controlled adhesion.

The authors are with the Robotics and Autonomous Systems Research Group, CSIRO, Brisbane, QLD 4069, Australia. Correspondence should be addressed to tirtha.bandy@csiro.au.

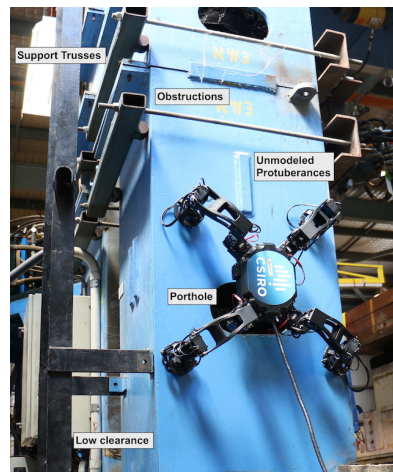


Fig. 1. Challenges faced by climbing robots in a typical industrial inspection scenario. The legged climbing robot, Magneto as shown in the scene, is built to explore open research questions of limited adhesion, whole-body planning and control, and complete coverage of complex 3D structures enabling the development of versatile climbing inspection robots.

Among platforms utilizing magnetic adhesion, various locomotion modalities have been explored. Tracked [12] and wheeled robots [9] are capable navigating smooth continuous surfaces like ship hulls with a high efficiency and low cost of transport. Articulation in the body structure allows such platforms to transition across planes of varying inclinations. However, tracked robots are not well suited for traversing sharp curvatures smaller than the wheel/track dimensions or negotiating beam edges. MagneBike [13] is an exception due to its innovative design which enables it to navigate across sharp beam angles and corners. However, like other wheeled and tracked platforms requiring continuous contact, MagneBike is still limited by its ability to traverse structural gaps. Legged platforms have the ability to negotiate structural gaps due to their ability to execute discontinuous contact transitions.

The simplest form of legged platform, a bipedal configuration, performing inchworm like locomotion has been explored successfully in navigating non-continuous surfaces. [14], [15] explored the idea of an inchworm like locomotion for complex structural navigation and demonstrated it traversing inverted and transitioning planar structures of varying inclination. [4] in addition proposed a multi-limbed version comprising of multiple “inchworm” type limbs. A more advanced version of inchworm configuration was developed in CROC [16], [17] where permanent magnets on each contact pads, manipulated using a patented adhe-

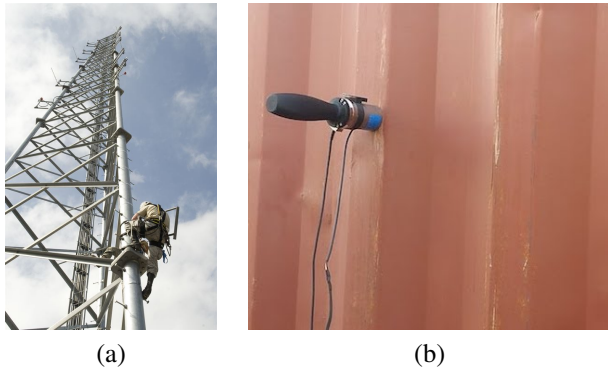


Fig. 2. Discontinuous surfaces of narrow width as seen in communication towers, seen in (a), and uneven surfaces seen on corrugated surface of a shipping container, as seen in (b), often limit the size of foot print available for adhesion. For scale comparison, a KEP magnet of width 40mm is attached to a ridge on the surface in (b). Wide footpads and tracks based robots become unusable for vertical locomotion on such surfaces.

sion mechanism, and 7-DOF body enabled the platform to perform complex maneuvers in traversing through narrow passages in the Sydney harbour bridge.

While the inchworm topology is an excellent configuration for minimal weight with high agility, it does not scale well with the requirement of heavier payloads and robot sizes. One of the key challenges of an inchworm topology is the requirement of a strong adhesion at the foot as the only a single adhesion surface balancing the cantilever serial-chain topology of the body during operation. This often requires a relatively large footpad to generate sufficient support moment. Large footpads are suitable for planar surfaces like wide structural elements and ship hulls, but have limited success on narrow beams often seen in structural elements in communication towers or many support trusses. Fig. 2 shows two typical scenarios where a small adhesion footprint is necessary due to the surface characteristics. Multi-limbed platforms are able to synthesize a much larger support polygon by carefully selecting suitable contact positions depending on the contact force requirement.

The idea of using multiple limbs to traverse vertical surfaces has been investigated for almost two decades. Quadruped robots like NINJA series [3], MRWALLSPECT [2], LEMUR-3 [18], hexapedal platforms like RiSE [5], REST [10], ASTERISK [19] are just a few representative of the enormous literature on the topic. A special mechanism in RISE [5] enables the platform to adapt its leg orientation to transition from horizontal to vertical surfaces. However, most of these multi-limbed platforms have traditionally been designed primarily to demonstrate climbing continuous surfaces (e.g wall climbing, or inverted walking) and have not been explicitly designed to undergo significant body deformations for traversing complex 3-D structures as shown in environments like Fig. 2(a).

While locomotion on vertical or inverted inclination is a hard task, performing highly dexterous and whole body maneuvers on such surfaces compounds the complexity even more. It requires ensuring that load on the adhesion surface does not exceed the adhesion limits. In addition, while indi-

vidual limbs can be controlled in a decentralized manner for a simple gait climbing control, as shown successfully by many multi-limbed climbing robots, a versatile body positioning requires whole body coupled planning and control to achieve non-trivial desired body configurations during inspection.

To motivate a typical scenario, let's examine Fig. 1 shows an inspection scenario fraught with navigation challenges to climbing robots. A truly robust versatile legged climbing robot would have to step over and inspect portholes and obstructions, squeeze under low clearance beams, walk on truss beams of various separations and inclinations to inspect the complete structure. These range of capabilities have not yet been demonstrated on a single platform.

To develop such versatility in climbing we have developed a novel magnetic foot quadruped platform, named Magneto. Magneto is designed specifically to provide enough limb workspace and limb manipulability while reducing the moments due to gravity on the contact points to enable traversing complex 3-D structures and achieving a wide range of body configurations for desired sensor positioning. Specifically, we show the platform's capability in several challenging scenarios

- traversing surfaces at any incline,
- traversing on narrow beams of various separation,
- ability to negotiating narrow spaces and
- ability to switch from locomotion to inspection of confined space voids.

Section II provides a detailed description of the adhesion mechanism (II-A), kinematic structure of the limb (II-B). The overall control system and gait generation described in Section II-C. The platform's performance is subsequently evaluated in detail in Section III.

II. SYSTEM DESCRIPTION

Magneto, is a quadruped robot with three degrees of freedom per leg that incorporates one Kanetec KEP-4C permanent electromagnets per leg as its method of adhesion. The foot print of each leg is 40mm, the diameter of the cylindrical magnet. Magneto's mass is 5.53 kg and 5.87 kg inclusive of the tether. While operational, magneto fits within a cuboid 660×600×320 mm and packs away into a 370×210×250 mm cuboid. Magneto's design allows flexibility in build as the foot, leg, and body are modular and can be altered in size and configuration quickly as a large portion of its components are 3D printed on common FDM machines. For the purposes identification in further sections of this paper, the legs will be identified clockwise from the front-right leg as AR, BR, BL and AL.

A. Adhesion mechanism

As a ferrous inspection surface can also act as a support surface in many inspection scenarios, magnetic adhesion was chosen for this robot prototype. However, the control, planning and design framework can be significantly reused for other adhesion mechanisms, eg, a suction cup. To enable the platform to attach to a ferromagnetic inspection surface,

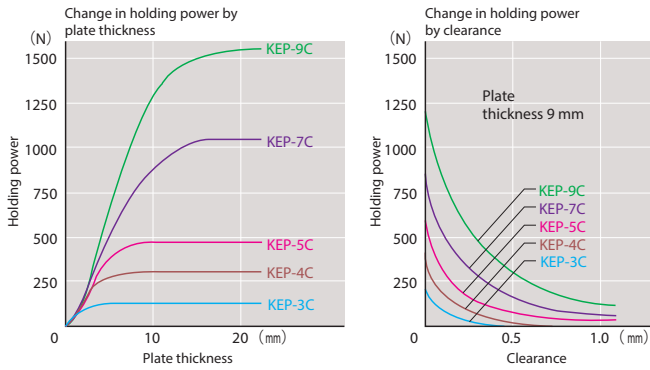


Fig. 3. Holding force of the Kanetec KEP magnet series vs plate thickness and clearance as provided in the manufacturer’s datasheet [20].

electromagnetic adhesion enabled by an electro-permanent-magnet was explored. An electro-permanent-magnet has a hard magnetic core that provides a fixed magnetic force while the soft magnetic material around the central core can be magnetized by an electrical current to augment or cancel the base magnetic force of the unit. Having permanently magnetized foot-tips reduces power consumption on stance or support legs while the robot is stationary and power is only consumed during the decoupling of the robot leg from the ferrous surface, which is a small fraction of the motion cycle, reduced the overall consumption of power significantly. Additionally, in the event of failure of electrical or control signal, the robot foot remains safely attached to the inspection surface.

Fig. 3 shows the holding force of the Kanetec KEP magnet series as a function of plate thickness and clearance. We validated by empirical testing that the adhesion force was sufficient for the whole robot body as well as the maximum length of the tether (3m in this prototype) for vertical locomotion. The separation force measured by an ATI-force torque sensor on the magnet was 147N. On the test-rig, in the quadruped configuration, Magneto can carry a payload of upto 1.5Kg strapped on its body while climbing vertically up, a task that induces the largest shear forces on the adhesion surface. Infact, the payload capacity is primarily a function of the adhesion forces that depends on the magnet strength and the surface properties. In general this can be drastically increased by using a stronger magnet e.g KEP-5C per limb or by increasing the number of limbs, although it should be noted that gains in adding more limbs are mitigated to an extent by the increased body weight and system complexity.

As compared to most ground robots with spherical foot tip models, foot tip placement for Magneto has additional constraints due to the requirement that the magnetic foottip be aligned with the surface normal and the fact that for gripping adhesion modes, the surface slip has to be avoided for stable locomotion. This, in turn, induces additional constraints on the foot tip movement. A special foot design described in Section II-B enables movement and compliance to the contact surface under such constraints.

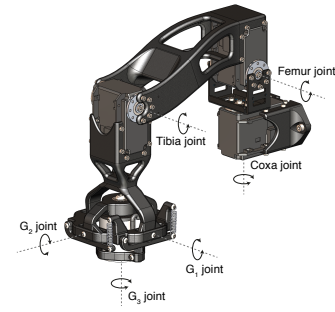


Fig. 4. CAD model of single leg showing all 6 DOF, 3 actuated and 3 passively compliant

B. Kinematic structure of each limb

Maintaining adhesion during the walking cycle is paramount to the success of a climbing robot. In order to adhere to the surface and locomote regardless of the adhesion type the robot requires a foot coupling able to gimbal about the adhesion point, minimising torques applied to the foot and ensuring there is no slip induced from the stance phase of the step cycle. Furthermore during the swing phase of the step cycle the magnet should be consistently aligned with the leg so that it can be placed on the surface in a repeatable manner.

To reduce overall robot complexity a passive self-centering gimbal was designed with small return to centre springs on each axis. The gimbal effectively creates a leg with 6DOF overall with the last 3DOF in the link chain being passively actuated with small spring forces satisfying the conditions for walking with adhesion. Shown in Fig. 4, the gimbal based foot holds at its centre the magnet, from the foot the G3 DOF rotates about the axis of the magnet $\pm 90^\circ$ an internal spring returns the magnet to its central position. Following are two consecutive perpendicular pivots, G2 and G1, both intersecting the centre axis of the magnet with a range of $\pm 30^\circ$ about centre position. The pivot point is at 31 mm from the base of the foot minimising the torque applied to the adhesion mechanism while allowing for clearance of the external gimbal assembly at full actuation. Both the G1 and G2 DOF are actuated by an easily tunable single spring mechanism that creates equal return torque independent of direction. It is important that the gimbal is a zero point gimbal as the 3DOF leg can only control a point in Cartesian space and not the tool tip pose. Attached to the foot is a hall-effect based proximity switch, a temperature sensor and a 6axis force torque sensor to monitor the state of the magnets and adhesion during locomotion.

Quadruped gaits offers quasi static stability while three or more feet are in an adhesion state. Magneto’s three DOF leg configuration allows the centre point of the gimbals to be controlled in Cartesian space within the leg’s allowable workspace. To maximise the foot’s workspace each leg is attached to the body at the corners facing 45° away from the robot’s Sagittal plane. In order to reduce the moment created by the body mass about the adhesion points while the robot is climbing a vertical wall, the leg is designed in a manner as

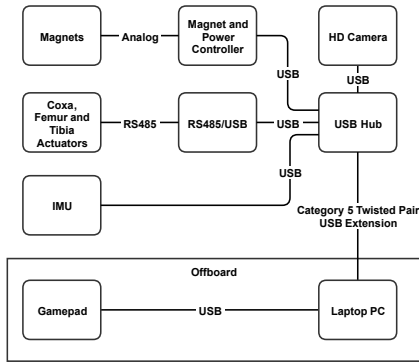


Fig. 5. System architecture of Magneto showing the sensing, actuation and controller connectivity

to keep the body as close as possible to the adhesion surface, thereby reducing gravitational moments, whilst maintaining an appropriate workspace as the foot gimbals. The ability to change the separation from the adhesion surface also allows Magneto to perform contact tests on sensors mounted on the underside of its central body frame. The Coxa joint directly intersects the axis of the Femur joint creating a 2DOF pivot point above the Coxa. This is primarily done to reduce the overall size of the robot while maintaining a large working range for the Coxa joint. The Femur joint has a large range of motion allowing the Femur joint to be moved through a greater than 180° arc. The Tibia joint also allows for 270° arc about its centre position. The combination of these joint limits offers a dexterous leg and overall dexterous robot.

The body of the robot houses the power and electrical systems. The system architecture is shown in Fig. 5. Encapsulation of electronics provides robustness to environmental hazards and incorporates cooling channels for the power systems. Internal to the robot is a Microstrain GX3 IMU and a custom-built magnet controller unit that controls the power cycle to the magnets as well as monitoring system health.

The robot is connected to a tether consisting of a data link as well as power. While adding a tether requires proper cable management during operation in complex 3D environments, the benefits often outweigh the hindrances. The tether allows the robot to operate for prolonged periods as it is not constrained by available power. A 24V power supply is used to supply the tether, a power management system conditions the power at the robot end of the tether, providing the necessary step down or up to the required operating voltage of each sub system on the robot, including 5V magnet controller and data link circuitry, 15.6V actuators, and 24V magnets. Monitoring of subsystem power status, consumption and temperatures are performed by the magnet controller circuitry. Overall, the tethered system provides the system with a higher degree of robustness and reliability compared to a fully autonomous untethered system. For this paper, we ignored aspects of load variations introduced by increasing tether length supported by the robot as it climbs,

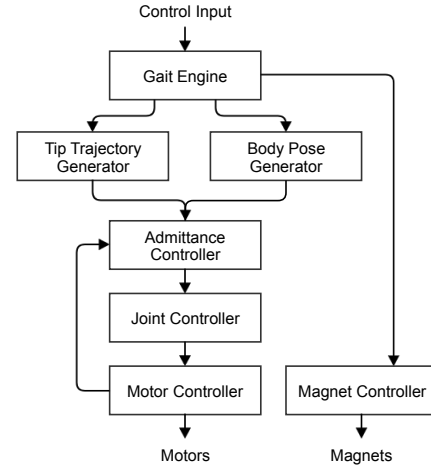


Fig. 6. Control architecture of Magneto showing the motor as well as magnetic adhesion control pathways.

as well as the drag effects of the tether on the surface. We instead ensured that the forces required for adhesion of the whole robot included the maximum load induced by the full tether held against gravity.

C. Control Architecture

The control architecture consists of a hierarchy of controllers (Fig. 6) which work together to ensure Magneto walks at a desired input velocity defined by the user whilst posing the body and legs such that the leg magnets adhere to the walking surface. The top level of the hierarchy is a gait engine which keeps time of a predefined gait pattern (Fig. 8) and outputs the state, either Swing or Stance, of the walk cycle for each leg. This leg dependent walk cycle state is the control variable for magnetisation/demagnetisation of the adhesion module such that the magnets are magnetised in the Stance state and demagnetised in the Swing state. These states are also fed to a tip trajectory engine and body pose generator which together generate an output desired tip position.

The generated desired tip trajectory will differ depending on the orientation of the walking surface and is generated from the combination of the output of the Tip Trajectory Engine and Body Pose Generator. The base tip trajectory from the Tip Trajectory Engine is generated to adhere to several key criteria, namely:

- C1 smooth at non-constant body velocity and C2 smooth at constant body velocity.
- A peak height at the middle of the Swing period defined by a 'Step Clearance' parameter, which for most experiments was set to 100mm.
- A stride length defined by the desired body velocity and constrained by calculated workspace boundaries for each leg.

This base trajectory can be seen in its original form in Fig. 7 which shows the leg trajectory (in the world frame) whilst in operation on a horizontal (0 degree) surface. For

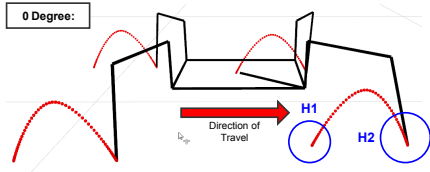


Fig. 7. Leg trajectories (in world frame) for 0° operation surface. H1: the beginning of the swing period where the tip magnet demagnetises and decouples from the walking surface. H2: the end of the swing period where the magnet is controlled to magnetise and adhere to the walking surface

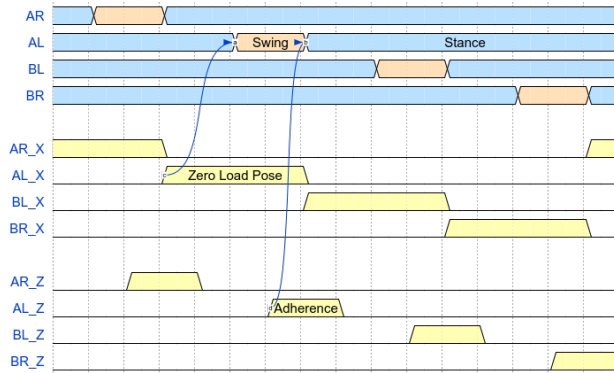


Fig. 8. Diagram detailing gait and leg pose timing example for traversing 90° plane. The Zero Load Pose and Adherence Pose periods are timed such that peak posing occurs during the start and end of the swing period respectively.

this operational mode further modification to the base leg trajectory was unwarranted, however, for more complex operational modes the base trajectory is modified via a desired body pose generated from the Body Pose Generator. The goal of the generated body pose is two fold and can be broken down into two distinct periods: the Zero Load Posing period and the Adherence Posing period.

The Zero Load Posing period is posing of the body that occurs before and during the start of the Swing period of a leg to minimise the load on the tip when the Swing phase starts and the magnet decouples from the surface. Fig. 8 shows the timing of such posing for a vertical (90°) surface operational mode. In this example, the Body Pose Generator generates a forward translation pose of the body and the next swinging leg, AR, which is rigidly posed with the body. Since this posing occurs before the start of the swing period, the leg is posed whilst the magnet is still coupled to the surface. This constrained posing induces a force at the tip and torques in the joints in opposition to those forces and torques which are the result of the load of the robot, the ultimate goal being the minimisation of any net forces and torques on the leg before the start of the swing period and demagnetisation of the magnet. Fig. 9 shows the desired tip trajectories, in the world frame, for Magneto walking on an operational surface at 90° and the section of the curve V1 shows the desired translation output from the Zero Load Posing period.

The second period of posing occurs toward the end of the swing period of each leg and is used to ensure the magnet at the leg tip adheres to the surface. Due to the inherent non-

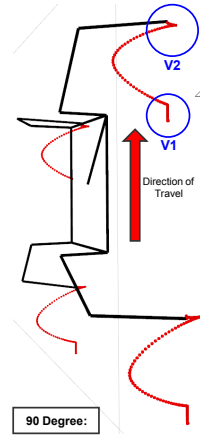


Fig. 9. Leg trajectories (in world frame) for 90° operation surface. (V1) Leg posing to minimise load on tip before initiating swing period. (V2) Leg posing to ensure magnet is in correct position/orientation at end of swing to make contact with, and adhere to walking surface.

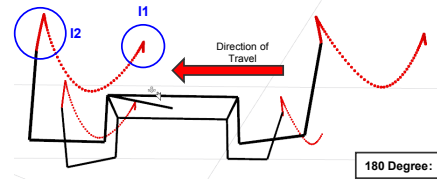


Fig. 10. Leg trajectories (in world frame) for 180° operation surface. (I1) Leg posing to minimise load on tip before initiating swing period. (I2) Leg posing to ensure magnet is in correct position/orientation at end of swing to make contact with, and adhere to walking surface.

rigidity of the system there is enough compliance in the joints and links that the actual tip position does not always reach the command position. For example, whilst operating inverted on a 180° surface, the tip would often fail to reconnect to the surface after completing the swing period due to the pull of gravity away from the walking surface. To compensate for this, the Adherence Pose period poses the body and the swing leg before and during the end of each swing period such that the tip successfully reconnects with the walking surface and ensures the magnet will adhere. In the I2 section of the trajectory of Fig. 10 it can be seen that Adherence Posing adjusts the base tip trajectory such that it travels further toward the walking surface. Once connected with the surface, after the swing period and adhering the magnet to the surface, the Adherence pose is relaxed. Adherence posing is also used in some operational modes to pose the tibia link orientation around in order to rock the gimbal holding the magnet into place thus ensuring a flush contact between magnet and surface which allows for adhesion.

III. PERFORMANCE CHARACTERISTICS

In order to characterise the platform performance, we first show the flexibility of the platform in achieving a given body configuration. This flexibility ensures that the platform is able to attain the desired body configurations as required while performing full body control. Subsequently, we test

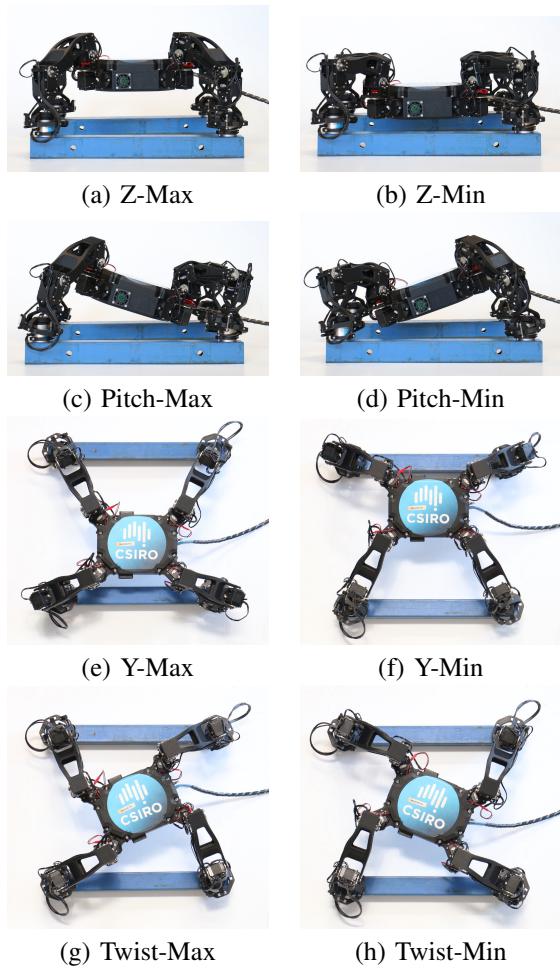


Fig. 11. (a-h) shows Magneto's limits of body posing for payload positioning.

TABLE I
THE LIMITS OF BODY POSITION IN PRIMARY DIMENSIONS.

Axis of Flexibility	Range
Longitudinal (x) Translation	± 75 mm
Lateral (y) Translation	± 75 mm
Height (z) Translation	± 40 mm
Roll (x) Rotation	± 0.25 rad
Pitch (y) Rotation	± 0.25 rad
Yaw (z) Rotation	± 0.4 rad

Magneto's capability in ability to walk at various inclinations and its ability to traverse on narrow beams in spite of varying separation and low clearance.

A. Limits of body positioning

Due to its high degrees of freedom, Magneto has significant flexibility in posing its torso to enable specific view point required by a payload, a specific configuration required for traversal of the environment or to enable stability using full body control. Table I shows the range of movements and Fig. 11 shows the body positioning in a few selected directions in a constrained configuration of the foot attached to a narrow beam.

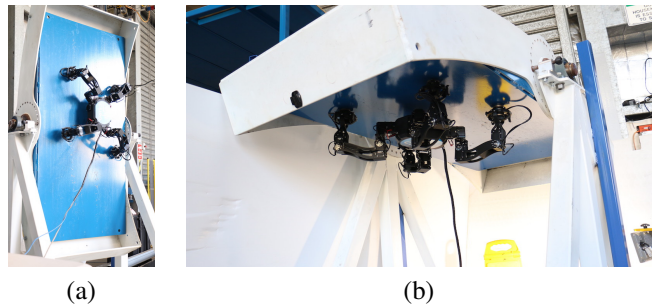


Fig. 12. Magneto traversing (a) vertical (90deg) and (b) inverted (180deg) surfaces

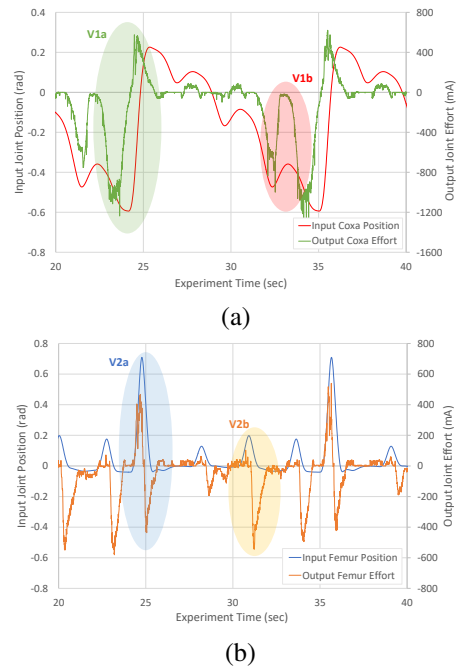
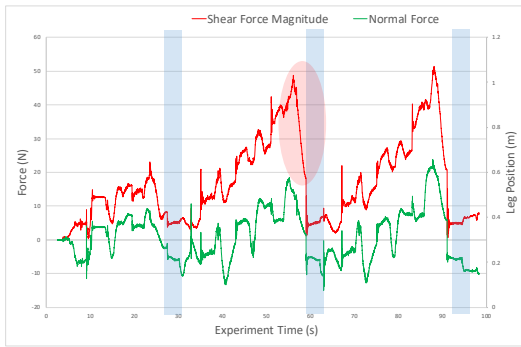


Fig. 13. Plots showing typical waveform of input joint position and resultant joint effort for Leg AR Coxa (a) and Femur (b) Joints during tests in a 90° operational mode. Highlighted are sections of the waveform which show the Zero Load Posing periods (V1a/b) and the Adherence Posing periods (V2a/b).

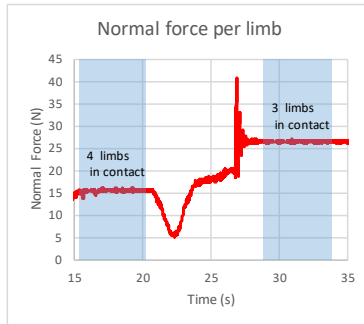
B. Traversing various inclination

Fig. 14 shows the forces measured on a 6-axis force torque sensor on a limb during operation. In Fig. 14(a) the red marked regions shows the effect of Zero Load Posing in reducing the shear load before the limb is detached. The blue bands are the durations when the instrumented limb is in swing phase. The average increase in the shear force is a result of a combination of the increased lateral force on the limb as the body moves towards it, as well as the spring on the magnet gimbal. The stress on the gimbal is released everytime the limb enters swing phase. The periodic cycle of the load on the limbs remains under the separation bounds.

In Fig. 14(b) the robot is held inverted (180 deg) and made to transition from a 4 limb contact to 3 limb contact by detaching one limb. As the limb is released and the body comes to a stationary pose, we see the net force on each limb



(a)



(b)

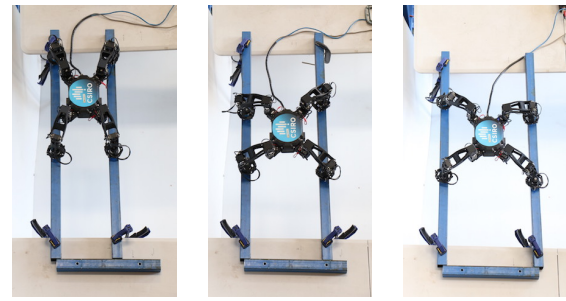
Fig. 14. Shear force and the normal force measured by a 6-axis ATI force-torque sensor on the AL limb during (a) a vertical (90 deg) climbing gait and (b) inverted (180 deg) limb detachment.

reaches to around 25N which is way below the separation value of 147N.

To test the robustness of the robot traversing at various inclinations, we designed a test-rig capable of rotating freely along the horizontal axis. Fig. 12 shows the rig at vertical and inverted configurations. While we are able to walk magneto at any angle, we show and discuss results for three primary inclinations, horizontal (0°), vertical (90°) and inverted (180°). The experiments were run over several iterations for 60 seconds each at a desired body velocity of 0.015m/s. The results of some of the experiments at 90° inclinations are shown in Fig. 13.

In the highlighted section V1a of Fig. 13 a), the result of the Zero Load Posing period can be seen, where the output torque of the coxa joint is minimised before the swing period begins at the 24 second mark. This functionality proved to be crucial to the successful operation of robot at 90° inclinations, as without this load minimisation the sudden transfer of load from the demagnetisation of the tip magnet at the beginning of each swing was enough to dislodge the remaining feet from the surface and cause a full robot disconnection from the walking surface.

In the highlighted section V2a of Fig. 13 b), the result of the Adherence Posing period can be seen. The spike in joint torque on the femur joint motor during the swing period is due to the connection of magnet and surface caused by the posing of the body (and rigidly connected swinging leg) toward the walking surface. The highlighted section V2b of the same figure shows the same joint motor again spiking



(a) 300 mm

(b) 400 mm

(c) 500 mm

Fig. 15. Magneto successfully traverses beams at different separations by adapting its gait parameters.

in torque during the same operation but for an adjacent leg making contact with the walking surface during its swing period.

C. Traversing narrow beams

Legged platforms can climb non-contiguous surfaces and we demonstrate the performance on a truss like test rig. The truss beams is quite challenging, with the available foot hold of 50mm cross section beams, for a robot foot of 40mm diameter. Our controller is able to maintain the accuracy of the footprint to remain within the tight bounds even with an open loop controller. We show the capability of the platform on 3 typical scenarios that the inspection robot has to adapt. With added perception module, the robot can then automatically choose a suitable foot separation and foot step size to adapt to a variety of truss like situations.

a) *Adapting to variable beam separation:* The nominal foot separation in an unrestricted environment is 400 mm. However, such separation is not guaranteed in a field environment and the robot has to adapt its footfall positions accordingly. While the platform can adapt its foot separation in a continuous manner, in this experiment Fig. 15 we demonstrate the ability of the platform to execute controlled footsteps on a narrow beam at three discrete settings of beam separation: 300 mm (Fig. 15a), 400 mm (Fig. 15b), 500 mm (Fig. 15c), each of which is successfully executed by the platform. As the foot positions diverge more from the nominal foot tip positions, the gimbals provide the required compliance for the magnet to align with the normal direction of the beams.

D. Adapting to low clearance

In addition to modifying its footprint, often the robot has to reduce its body separation from the adhesion surface to squeeze through a low clearance. Such a scenario is seen in Fig. 1 at the bottom left where a low clearance is created by structural beams. In this experiments we simulate such a scenario and show that the platform is able to reduce its body height to safely traverse a low clearance section. Fig. 16(a-d) shows a run where the robot is traversing a gap of 230 mm. The robot can squeeze through clearances as low as 200 mm.

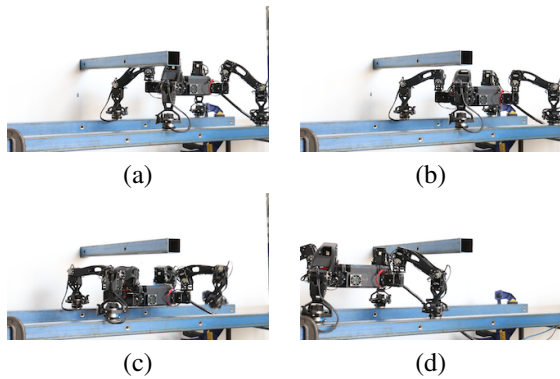


Fig. 16. Lowering body configuration to clear an obstruction with a maximum available clearance of 230 mm

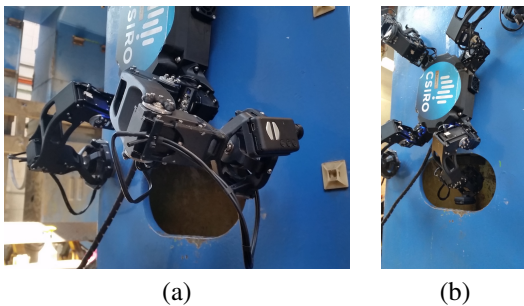


Fig. 17. Due to the design of its limbs and the control architecture, Magneto is able to seamlessly switch from locomotion mode to inspection mode. (a) shows Magneto's limb with a camera attached. (b) shows Magneto manipulating its limb to the interior of the structure through the porthole mid-climb.

E. Limb manipulation for inspection of portholes

A key advantage of multi-limbed high DOF robots is that the limbs can be used both for locomotion as well as inspection, even concurrently. Fig. 17 shows snapshots of such an operation. Assuming a tripod holding position, Magneto is able to detach one of the limbs to act as an inspection manipulator and probe the inside of the inaccessible porthole.

IV. CONCLUSION

In this paper, we presented a novel magnetic foot quadruped robot, Magneto, built to address open challenges that still exist hindering the deployment of a truly versatile climbing robot. By virtue of its novel design and control strategies, Magneto is capable of navigating any incline, traversing thin beams of various separation as well as squeezing through narrow clearances by deforming its body configuration. Exploiting its high redundancy, Magneto is able to switch between the use of its limbs from locomotion to localized inspection of hidden pockets in a seamless manner. Current improvements underway includes integrating a 3-D perception module on the platform for autonomous footfall placement and navigation on 3-D trusses. While there has been numerous climbing robots developed for inspection, Magneto is among the first robots to develop and demonstrate key capabilities relevant to climbing complex 3-D structures on a single platform.

REFERENCES

- [1] J. Nikolic, M. Burri, J. Rehder, S. Leutenegger, C. Huerzeler, and R. Siegwart, "A uav system for inspection of industrial facilities," in *Aerospace Conference, 2013 IEEE*. IEEE, 2013, pp. 1–8.
- [2] H. Kim, T. Kang, H. Choi, and S. Jangan-gu, "Walking and climbing robot for locomotion in 3d environment," in *International Symposium on Automation and Robotics in Construction, ISARC*, 2004.
- [3] A. Nagakubo and S. Hirose, "Walking and running of the quadruped wall-climbing robot," in *Robotics and Automation, 1994. Proceedings., 1994 IEEE International Conference on*. IEEE, 1994, pp. 1005–1012.
- [4] R. L. Tummala, R. Mukherjee, N. Xi, D. Aslam, H. Dulimarta, J. Xiao, M. Minor, and G. Danghi, "Climbing the walls," *Robotics and Automation Magazine*, vol. 9, no. 4, pp. 10–19, 2002.
- [5] M. Spenko, G. C. Haynes, J. Saunders, M. R. Cutkosky, A. A. Rizzi, R. J. Full, and D. E. Koditschek, "Biologically inspired climbing with a hexapedal robot," *Journal of Field Robotics*, vol. 25, no. 4-5, pp. 223–242, 2008.
- [6] S. Kim, A. T. Asbeck, M. R. Cutkosky, and W. R. Provancher, "Spinybot: climbing hard walls with compliant microspines," in *Advanced Robotics, 2005. ICAR'05. Proceedings., 12th International Conference on*. IEEE, 2005, pp. 601–606.
- [7] O. Unver, A. Uneri, A. Aydemir, and M. Sitti, "Geckobot: A gecko inspired climbing robot using elastomer adhesives," in *Robotics and Automation, 2006. ICRA 2006. Proceedings 2006 IEEE International Conference on*. IEEE, 2006, pp. 2329–2335.
- [8] B. Aksak, M. P. Murphy, and M. Sitti, "Gecko inspired micro-fibrillar adhesives for wall climbing robots on micro/nanoscale rough surfaces," in *Robotics and Automation, 2008. ICRA 2008. IEEE International Conference on*. IEEE, 2008, pp. 3058–3063.
- [9] J. Shang, B. Bridge, T. Sattar, S. Mondal, and A. Brenner, "Development of a climbing robot for inspection of long weld lines," *Industrial Robot: An International Journal*, vol. 35, no. 3, pp. 217–223, 2008.
- [10] J. C. Grieco, M. Prieto, M. Armada, and P. G. De Santos, "A six-legged climbing robot for high payloads," in *Proceedings of the 1998 IEEE International Conference on Control Applications*, vol. 1. IEEE, 1998, pp. 446–450.
- [11] K. H. Cho, Y. H. Jin, H. M. Kim, H. Moon, J. C. Koo, and H. R. Choi, "Multifunctional robotic crawler for inspection of suspension bridge hanger cables: Mechanism design and performance validation," *IEEE/ASME Transactions on Mechatronics*, vol. 22, no. 1, pp. 236–246, Feb 2017.
- [12] W. Shen, J. Gu, and Y. Shen, "Permanent magnetic system design for the wall-climbing robot," *Applied Bionics and Biomechanics*, vol. 3, no. 3, pp. 151–159, 2006.
- [13] F. Tâche, W. Fischer, G. Caprari, R. Siegwart, R. Moser, and F. Mondada, "Magnebike: A magnetic wheeled robot with high mobility for inspecting complex-shaped structures," *Journal of Field Robotics*, vol. 26, no. 5, pp. 453–476, 2009.
- [14] K. Kotay and D. Rus, "The inchworm robot: A multi-functional system," in *Autonomous Robots*, vol. 8, 2000, pp. 53–69.
- [15] A. Mazumdar and H. H. Asada, "Mag-foot: A steel bridge inspection robot," in *2009 IEEE/RSJ International Conference on Intelligent Robots and Systems*, Oct 2009, pp. 1691–1696.
- [16] P. Ward, P. Quin, D. Pagano, C.-H. Yang, D. Liu, K. Waldron, G. Dissanayake, G. Paul, P. Brooks, P. Mann, W. Kaluarachchi, P. Manamperi, and L. Matkovic, "Climbing robot for steel bridge inspection: Design challenges," in *9th Austroads Bridge Conference, Sydney*, 2014.
- [17] D. Pagano and D. Liu, "An approach for real-time motion planning of an inchworm robot in complex steel bridge environments," in *Robotica*, vol. 35, 2017, pp. 1280–1309.
- [18] A. Parness, N. Abcouwer, C. Fuller, N. Wiltzie, J. Nash, and B. Kennedy, "Lemur 3: A limbed climbing robot for extreme terrain mobility in space," in *International Conference on Robotics and Automation (ICRA) Singapore*. IEEE, 2017.
- [19] P. Kriengkamol, K. Kamiyama, M. Kojima, M. Horade, Y. Mae, and T. Arai, "New tripod walking method for legged inspection robot," in *2016 IEEE International Conference on Mechatronics and Automation*, Aug 2016, pp. 1078–1083.
- [20] "Model kep permanent electromagnetic holder," http://kanetec.co.jp/cgi-bin/catalog/catalog_en.cgi?alphabet=ke, accessed: 2017-09-15.